Water Practice & Technology Vol 14 No 3
doi: 10.2166/wpt.2019.052

Defluoridation of calcium-rich groundwater using iron oxide nanoparticles

Madhusha Sudasinghe, Mahesh Jayaweera*, Buddhika Gunawardana, Jagath Manatunge and Gayan Madhusanka

Department of Civil Engineering, University of Moratuwa, Moratuwa, Sri Lanka

*Corresponding author. E-mail: mahesh@uom.lk

Abstract

It has been suggested that moderate to high fluoride ion concentrations in the presence of calcium in groundwater can represent human health hazards resulting in possible lesions in tubular cells, leading to chronic kidney disease of unknown etiology (CKDu). This study focuses on fluoride removal in the presence of calcium using iron oxide nanoparticles (FeONs) as an effective adsorbent in single- and multi-solute batch-studies. Fluoride and calcium removal by FeONs in single-solute batch-studies occurred only by adsorption. Both species followed the Langmuir isotherm model and pseudo second-order kinetics, indicating monolayer adsorption and chemisorption, respectively. In multi-solute batch-studies, fluoride removal was attributed to adsorption and chemical precipitation forming CaF_2 in almost similar magnitude. For calcium removal in multi-solute studies, adsorption, co-precipitation, and precipitation were the prominent mechanisms, with co-precipitation dominant. Thus, FeONs are effective in fluoride removal by adsorption in both the presence and absence of calcium. FeONs could also be used successfully year-round in tropical climates, where calcium levels vary substantially, to lessen the risk of CKDu.

Key words: adsorption, calcium, CKDu, co-precipitation, fluoride, precipitation

INTRODUCTION

People drink groundwater containing substantial levels of fluoride (Chandrajith *et al.* 2012; Weragoda & Kawakami 2017), exceeding that recommended by the World Health Organisation (1.5 mg/L) (WHO 2017). Fluoride and its interactions with some other ions have been implicated as trigger factors of the 'chronic kidney disease of unknown etiology' (CKDu) prevalent in Sri Lanka (Wasana *et al.* 2016; Dissanayake & Chandrajith 2017; Dharma-wardana 2018). Over-extraction of groundwater, particularly during dry spells in tropical climates is highly likely to result in elevated fluoride and calcium levels. High calcium concentrations instigate a profound synergistic effect with fluoride on CKDu (Wasana *et al.* 2016). Fluoride exerts direct and calcium dose-dependent cytotoxic effects on human renal proximal tubular epithelial cells, and extracellular calcium chelation markedly attenuates fluoride-induced cell–death (Zager & Iwata 1997). The oxidative stress instigated by fluoride on human kidney cells also induces apoptosis and promotes the production of reactive oxygen species (anion superoxide, hydrogen peroxide, peroxynitrite, hydroxyl radicals), resulting in decreased cellular antioxidant defence mechanisms against oxidative kidney cell damage (Barbier *et al.* 2010).

Since about 2010, many researchers have studied fluoride removal using adsorption (Bhatnagar *et al.* 2011; Jayarathna *et al.* 2015), precipitation (Jadhav *et al.* 2015), ion exchange (Robshaw *et al.* 2019), electrodialysis (Belkada *et al.* 2018), coagulation and microfiltration (Da Conceição *et al.* 2015), and membrane filtration (Camacho *et al.* 2013). Among these, defluoridation using

Water Practice & Technology Vol 14 No 3
doi: 10.2166/wpt.2019.052

nanomaterial-based adsorption has gained considerable attention because of its efficiency. In particular, iron oxide nanoparticles (FeONs) have been widely studied (Raul *et al.* 2012). FeONs often favour fluoride and calcium adsorption, but the effect of calcium on defluoridation using FeONs does not appear to have been reported in the literature. In this study, the defluoridation potential of FeONs in both calcium-free and -rich groundwater was investigated. The study mainly focused on the different removal mechanisms of fluoride and calcium, adsorption isotherms, and kinetic studies of fluoride and calcium, using single- and multi- solute batch experiments.

MATERIALS AND METHODS

Synthesis and characterisation of FeONs

Nano zero-valent iron was synthesised following the modified method of Petala *et al.* (2013), using 0.18 M $FeCl_3$ and 0.94 M $NaBH_4$. FeONs were synthesised by purging compressed air (3.5 L/min) through the solution containing nano zero-valent iron particles. Finally, they were extracted by centrifuging, rinsing three times with ethanol and oven drying at 80 °C (Gui *et al.* 2012).

The morphology and elemental composition of the FeONs were analysed, before and after the adsorption experiments, using Environmental Scanning Electron Microscopy (ESEM, Carl Zeiss, EVO 18, Secondary Electron Microscope, Germany) coupled with Energy-Dispersive X-ray Spectroscopy (EDAX, Element EDS system, AMETEK Materials Analysis Division, USA). FeON phase identification was performed by X-ray Powder Diffraction (XRD-D8, ECO, Advance Bruker Diffractometer with filtered Cu Kα radiation, Germany). Fourier transform-infrared spectroscopy (FT-IR, ALPHA Bruker, Germany) was performed in adsorption mode at ambient temperature in the spectral range 500 to 4,000 cm^{-1} to identify the FeONs' functional groups.

Single-solute batch-studies for fluoride and calcium removal

Single-solute batch experiments were carried out to determine the FeON dosage at which maximum fluoride and calcium removal occurred (optimum FeON dosage). Dosage was varied from 0.04 to 7.20 g/L on the basis of preliminary studies. The operating parameters were – sample volume, 100 mL; contact time, 1 hour; initial fluoride and calcium concentrations, 5 and 300 mg/L, respectively; initial pH, 6.5; temperature, 28 °C; and, stirring speed, 150 rpm. The FeON dosage for maximum removal of fluoride and calcium was determined as 1.25 g/L. Subsequently, a series of batch experiments was conducted using the optimum FeON dosage, to determine the fluoride and calcium adsorption isotherm and kinetic behaviour. In these studies, the initial concentrations of fluoride and calcium were varied from 1 to 20 mg/L, and 100 to 500 mg/L, respectively. All other experimental conditions were similar to those used when determining the optimum FeON dosage. The theoretical amounts of fluoride and calcium adsorbed at equilibrium, $(Q_e)_{ad}$ and the actual amounts removed, $(Q_e)_{exp}$, were calculated to determine the extent of chemical precipitation and co-precipitation.

Multi-solute batch-studies for removal of fluoride and calcium

Multi-solute batch experiments were carried out in the presence of both fluoride and calcium to determine the optimum FeON dosage for maximum removal of fluoride and calcium. The operating parameters used were similar to those used in the single-solute batch studies and the optimum FeON dosage was determined as 1.25 g/L.

The differing amounts of fluoride and calcium removed by co-precipitation, chemical precipitation and adsorption were estimated by varying their respective concentration combinations. In CKDu

Water Practice & Technology Vol 14 No 3
doi: 10.2166/wpt.2019.052

prevalent areas in Sri Lanka, higher concentrations of fluoride and calcium have been reported during the dry season (June to August) than in the wet season. The combinations of fluoride and calcium concentrations considered for the multi-solute studies were based on seasonal variations typically encountered in the dry season. Twenty groundwater samples were collected during the dry season and the fluoride (1.1 to 9.0 mg/L) and calcium (140.0 to 900.0 mg/L) concentrations determined. Based on prevailing conditions in the CKDu affected areas, the experimental fluoride and calcium concentrations were set in the ranges 0.9 to 9.2 and 136.0 to 980.0 mg/L, respectively, and 10 fluoride/calcium concentration combinations were prepared accordingly. The concentration ranges were determined to exceed the natural equivalents slightly.

The first fluoride/calcium combination (0.9 and 136 mg/L, respectively) was prepared without FeONs and kept under quiescent conditions for 24 hours at ambient temperature to allow CaF_2 precipitation. After 24 hours, the mixture was filtered (Whatman™ 1003-110 Grade 3, 6 μm) and the residual fluoride concentration in the filtrate determined. FeONs (1.25 g) were subsequently added to 100 mL of the filtrate, and the mixture stirred continuously (150 rpm) at ambient temperature. The solution's residual fluoride and calcium concentrations were determined after one-hour contact time. The mixture's pH was monitored continuously for 72 hours. It always exceeded 5, confirming that no CaF_2 dissolution occurred. The same procedure was followed for all other fluoride/calcium combination solutions.

For different fluoride/calcium combinations without FeON, fluoride supersaturation levels were estimated and compared with the respective residual fluoride concentrations, to determine whether or not chemical precipitation had occurred, and estimate the quantities of CaF_2 precipitated. The solubility product (K_{sp}) of CaF_2 [$K_{sp} = (Ca^{2+})\ (F^{-})^2$], which is 3.5×10^{-11} $(mol/L)^2$ at 25 °C (Nasr *et al.* 2014), was used to determine fluoride supersaturation levels for different calcium concentrations. XRD and ESEM-EDX analyses were performed to confirm CaF_2 precipitation, and the quantities used to estimate the corresponding amounts of fluoride and calcium precipitated. The amounts of fluoride and calcium adsorbed onto FeONs were estimated assuming monolayer adsorption phenomena. As the amounts of fluoride and calcium both adsorbed and precipitated were known, the amounts co-precipitated were estimated from the total amounts of these species removed from solution.

Analysis of fluoride and calcium

Residual fluoride concentrations were analysed by ion chromatography (Metrohm, 930 Compact IC Flex, Switzerland) with a mobile phase of 3.2 mmol/L Na_2CO_3 + 1 mmol/L $NaHCO_3$, and a flow rate of 0.7 m/L/min. Residual calcium concentrations were determined using the EDTA titrimetric method based on USEPA Method No. 130.2 (USEPA 1983). Deionised water (18.2 Ω/cm) from a deioniser (Smart Plus-N, Heal Force, China) was used in all experiments.

Adsorption isotherms and kinetic studies for fluoride and calcium removal

Single-solute batch-studies

The experimental data were used to study fluoride and calcium removal with adsorption isotherms and kinetic models. The amount of fluoride or calcium removed per unit mass of FeONs (Q_e in mg/g) for a single solute was calculated using Equation (1):

$$Q_e = (C_o - C_e) \times \frac{V}{W} \quad (1)$$

where C_o and C_e are the initial and equilibrium concentrations of fluoride or calcium in solution (mg/L) respectively, V the volume of solution (L), and W the mass of the adsorbent (g).

Water Practice & Technology Vol 14 No 3
doi: 10.2166/wpt.2019.052

The Langmuir adsorption isotherm model was used to study fluoride and calcium removal and describe the amount of adsorbate adsorbed per unit weight of adsorbent at equilibrium. The Langmuir model is based on the assumptions that the adsorbent surface is homogeneous with equal sorption sites, only monolayer adsorption occurs with no interaction between adjacent adsorbed ions, and adsorbate ions tend to either adsorb or desorb. The isotherm (Langmuir 1918) is represented by Equation (2):

$$\frac{1}{Q_e} = \frac{1}{Q_m} + \frac{1}{Q_m K_L C_e} \tag{2}$$

where C_e is the equilibrium concentration of adsorbate (mg/L), Q_e the amount of adsorbate adsorbed per unit mass of adsorbent at equilibrium (mg/g), Q_m the maximum monolayer coverage capacity (mg/g), and K_L the Langmuir isotherm constant (L/mg). The dimensionless constant separation factor or equilibrium parameter, R_L, as given in Equation (3) is used to express the essential characteristics of the Langmuir adsorption isotherm:

$$R_L = \frac{1}{[1 + (1 + K_L C_o)]} \tag{3}$$

where C_o is the initial concentration (mg/L) and K_L the Langmuir isotherm constant. R_L describes the adsorption mechanisms – i.e., unfavourable ($R_L > 1$), linear ($R_L = 1$), favourable ($0 < R_L > 1$), or irreversible ($R_L = 0$) (Weber & Chakravorti 1974).

The Freundlich model was applied for fluoride and calcium removal to ascertain the adsorption characteristics. It is based on an assumption of heterogeneous surfaces where fluoride or calcium could bind by multi-layer formation, with interaction among adsorbed ions. The isotherm (Freundlich 1906) is represented by Equation (4):

$$\log (Q_e) = \log (K_f) + \frac{1}{n} \log (C_e) \tag{4}$$

where K_f is the Freundlich isotherm constant (mg/g), n the adsorption intensity, C_e the equilibrium concentration of the adsorbate (mg/L), and Q_e the amount of adsorbate adsorbed per gram of adsorbent at equilibrium (mg/g). The Freundlich constant (n) indicates the adsorption mechanism; when $2 < n < 10$, adsorption is favourable, between $1 < n < 2$ it is moderately difficult and when $n < 1$ adsorption is poor (Kakavandi *et al.* 2013).

The experimental data for fluoride and calcium were fitted to the Brunauer-Emmett-Teller (BET) adsorption isotherm model, based on the postulation of adsorption in the form of multilayers but without interaction between adsorbed ions. The isotherm describes the adsorption of multiple ions at each site, energetically homogeneous adsorption sites with no adsorbate interactions between neighboring ions, and immobile adsorbed ions. The BET isotherm (Brunauer *et al.* 1938) is given by Equation (5):

$$\left[\frac{C_e}{(C_s - C_e) \times Q_e}\right] = \left(\frac{K_B - 1}{K_B \times Q_o}\right) \times \frac{C_e}{C_s} + \frac{1}{(K_B Q_o)} \tag{5}$$

where C_e is the equilibrium concentration (mg/L), C_s the adsorbate monolayer saturation concentration (mg/L), Q_o the maximum adsorption capacity for forming single layers (mg/g), and K_B the BET adsorption isotherm which relates to the energy of surface interaction (L/mg).

The experimental data were fitted to the Dubinin-Radushkevich isotherm, which is generally applied to express the adsorption mechanism with a Gaussian energy distribution onto a heterogeneous surface, distinguishing between chemisorption and physical adsorption (physisorption)

Water Practice & Technology Vol 14 No 3
doi: 10.2166/wpt.2019.052

(Dubinin 1960) – see Equation (6):

$$\ln Q_e = \ln Q_d - B_D \varepsilon^2 \tag{6}$$

where Q_e is the amount of adsorbate in the adsorbent at equilibrium (mg/g), Q_d the theoretical isotherm saturation capacity (mg/g), B_D the Dubinin-Radushkevich isotherm constant (mol^2/kJ^2), and ε the potential energy (estimated using Equation (7)). E is the Dubinin-Radushkevich isotherm constant (kJ/mol) and can be estimated using Equation (8). Physisorption is likely if $E < 8$ kJ/mol, chemisorption if $8 < E < 16$ kJ/mol, and stronger chemical adsorption over ion exchange if $E > 16$ kJ/mol.

$$\varepsilon = RT \ln \left[1 + \left(\frac{1}{C_e}\right)\right] \tag{7}$$

$$E = \frac{1}{\sqrt{2 B_D}} \tag{8}$$

The fluoride and calcium data were also fitted to the Temkin adsorption isotherm (Tempkin & Pyzhev 1940), which contains a factor that considers adsorbent-adsorbate interactions explicitly. The isotherm is given by Equations (9) and (10):

$$Q_e = \left(\frac{RT}{b}\right) \ln A_T + \left(\frac{RT}{b}\right) \ln C_e \tag{9}$$

$$\mathrm{B} = \left(\frac{RT}{\mathrm{b}}\right) \tag{10}$$

where A_T is the Temkin isotherm equilibrium binding constant (L/g), b the Temkin isotherm constant, R the universal gas constant (8.314 J/mol/K), T temperature (K), and B a constant related to the heat of sorption (J/mol).

The kinetics of fluoride and calcium adsorption were analysed using Lagergren's pseudo-first-order kinetic model (Lagergren 1898), which describes the adsorption of one ion of adsorbate onto one adsorption site, and the pseudo-second-order kinetic model, which describes the adsorption of one ion of adsorbate onto two adsorption sites (Ho & McKay 1999). These two models identify the fluoride and calcium adsorption process kinetics to be fitted to either chemisorption or physisorption. The pseudo-first order and pseudo-second-order kinetic models are expressed in Equations (11) and (12):

$$\log\ (Q_e - Q_t) = \log\ Q_e - \left(\frac{K_1}{2.303}\right) t \tag{11}$$

$$\frac{t}{Q_t} = \frac{1}{[K_2\ (Q_e)^2]} + \left(\frac{1}{Q_e}\right) t \tag{12}$$

where Q_e is the amount of adsorbate adsorbed on the adsorbent (mg/g) at equilibrium, Q_t the amount of adsorbate adsorbed (mg/g) at time t (minutes), K_1 the rate constant (min^{-1}) for pseudo-first-order kinetics, and K_2 the rate constant (gm/g/min) for pseudo-second-order kinetics.

Multi-solute batch-studies

The extension of the Langmuir equation proposed by Jain & Snoeyink (1973) was applied to determine the monolayer adsorption of binary mixtures consisting of fluoride and calcium by FeONs,

Water Practice & Technology Vol 14 No 3
doi: 10.2166/wpt.2019.052

with competitive adsorption of the binary mixtures. This development was based on the assumption that only a fraction of the active adsorption sites available for fluoride could also be occupied by calcium. The amounts of fluoride or calcium adsorbed on FeONs are estimated using Equations (13) and (14):

$$q_1 = \frac{(Q_{m,1} - Q_{m,2})b_1c_1}{1 + b_1c_1} + \frac{Q_{m,2}\, b_1c_1}{1 + b_1c_1 + b_2c_2} \tag{13}$$

$$q_2 = \frac{Q_{m,2}\, b_2c_2}{1 + b_1c_1 + b_2c_2} \tag{14}$$

where $Q_{m,1}$ is the adsorption capacity of adsorbate-1 (fluoride) at equilibrium under single-solute study (mg/g); and b_1 and c_1 the Langmuir isotherm constants for adsorbate-1 under single-solute study (L/mg), and the equilibrium concentration of adsorbate-1 obtained under single-solute study (mg/L), respectively. The symbols incorporating suffix 2 have the same meanings as those with suffix 1 but ascribed to adsorbate-2 (calcium).

Fluoride and calcium supersaturation are a prerequisite for CaF_2 precipitation (Nath & Dutta 2010). Thus, fluoride removal depends on both the calcium concentration and the initial fluoride concentration, implying lower likelihood of precipitation for low initial fluoride concentrations.

The average FeON crystallite size was calculated from the XRD spectrum using the Scherrer Formula – Equation (15) (Chekli *et al.* 2016):

$$D = \frac{0.9\lambda}{\beta \cos\theta} \tag{15}$$

where D is the average crystallite size, λ the wavelength of the X-ray radiation, β the full width of the half maximum diffraction peak, and Θ the angle of diffraction.

RESULTS AND DISCUSSION

Characterisation of FeONs

XRD analysis

Figure 1(a) shows the XRD spectrum of synthesised FeONs, exhibiting peaks at 30.4°, 35.8°, 43.7°, 57.6°, and 63.1°, which correspond to diffraction of the (220), (311), (400), (511), and (440) planes,

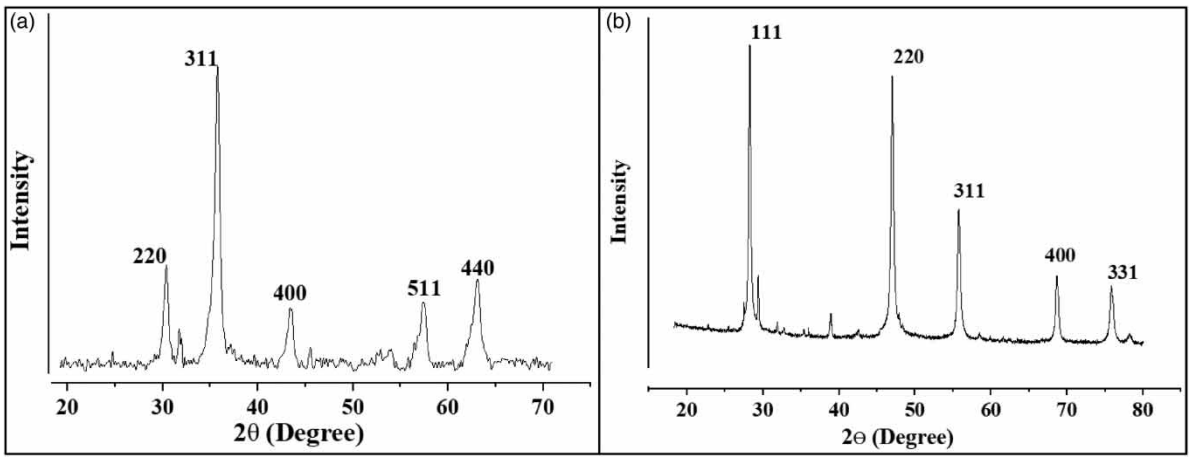

Figure 1 | XRD spectra of (a) synthesised FeONs and (b) CaF_2 formed in the aqueous solution.

Water Practice & Technology Vol 14 No 3
doi: 10.2166/wpt.2019.052

respectively, of magnetite nanoparticles. Others have made similar observations for XRD characterisation (Lin *et al.* 2005; Xu *et al.* 2007; Wu *et al.* 2011; Raul *et al.* 2012; Mohseni-Bandpi *et al.* 2015; Shukla *et al.* 2015). The average crystallite size obtained for this study was 46.3 nm, confirming that a significant fraction of FeONs was within the nano-scale range. XRD analysis [Figure 1(b)] of CaF_2 shows peaks at 28.2° (111), 46.9° (220), 55.7° (311), 68.6° (400) and 75.8° (331), confirming the formation of CaF_2 precipitate (Pandurangappa *et al.* 2010; Tahvildari *et al.* 2012) in the binary mix, with the average particle size 96.3 nm.

ESEM–EDX analysis

The ESEM image of synthesised FeONs (Figure 2(a)) shows the presence of interlinked flake-like aggregates, indicating agglomeration, possibly because of magnetic interaction between particles.

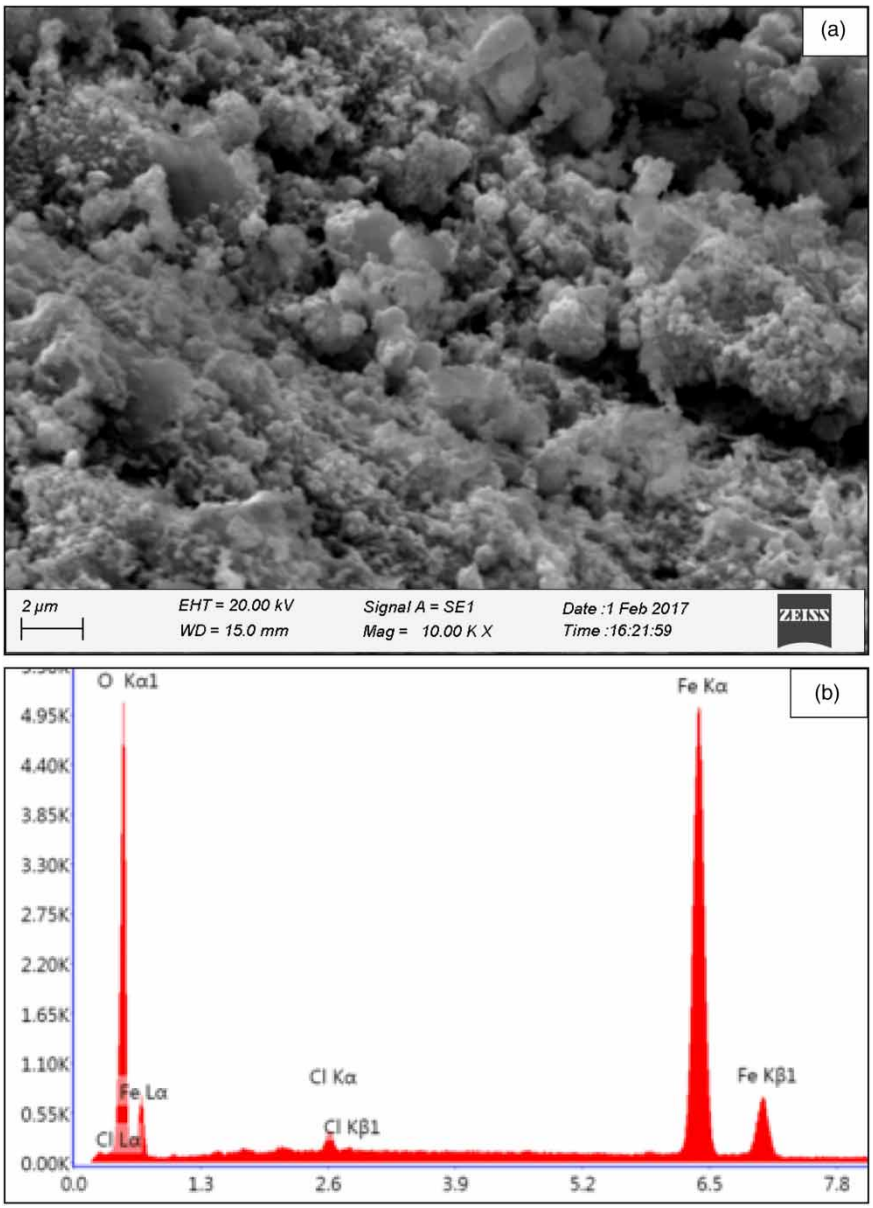

Figure 2 | (a) ESEM image of FeONs and (b) EDX spectrum of FeONs (*Note*: EDX was performed on the whole surface area in Figure 2(a)).

Water Practice & Technology Vol 14 No 3
doi: 10.2166/wpt.2019.052

The EDX analysis (Figure 2(b)) shows that the surface was composed of Fe and O with no impurities, and the narrow diffraction peaks confirm the crystalline structure. Similar observations on the agglomeration and crystalline structure formation of FeONs are reported by Lin *et al.* (2005) and Azzam *et al.* (2016). ESEM analysis of FeONs after fluoride adsorption in single-solute batch-studies shows spherical agglomerated particles with sharp edges (Figure 3(a)) and EDX analysis confirms the presence of fluoride adsorbed on FeON surfaces (Figure 3(b)). Figure 4(a) depicts the morphology of the FeON surface after multi-solute batch-studies, where both fluoride and calcium adsorbed and co-precipitated, which are visible as fluffy and irregular shapes. A magnified ESEM image (nm-scale) shows a nodular-like pattern on the FeON surface, which is ascribed to calcium co-precipitation with FeONs (Figure 4(b)). EDX analysis confirmed the presence of both fluoride and calcium on the FeON surface (Figure 4(c)).

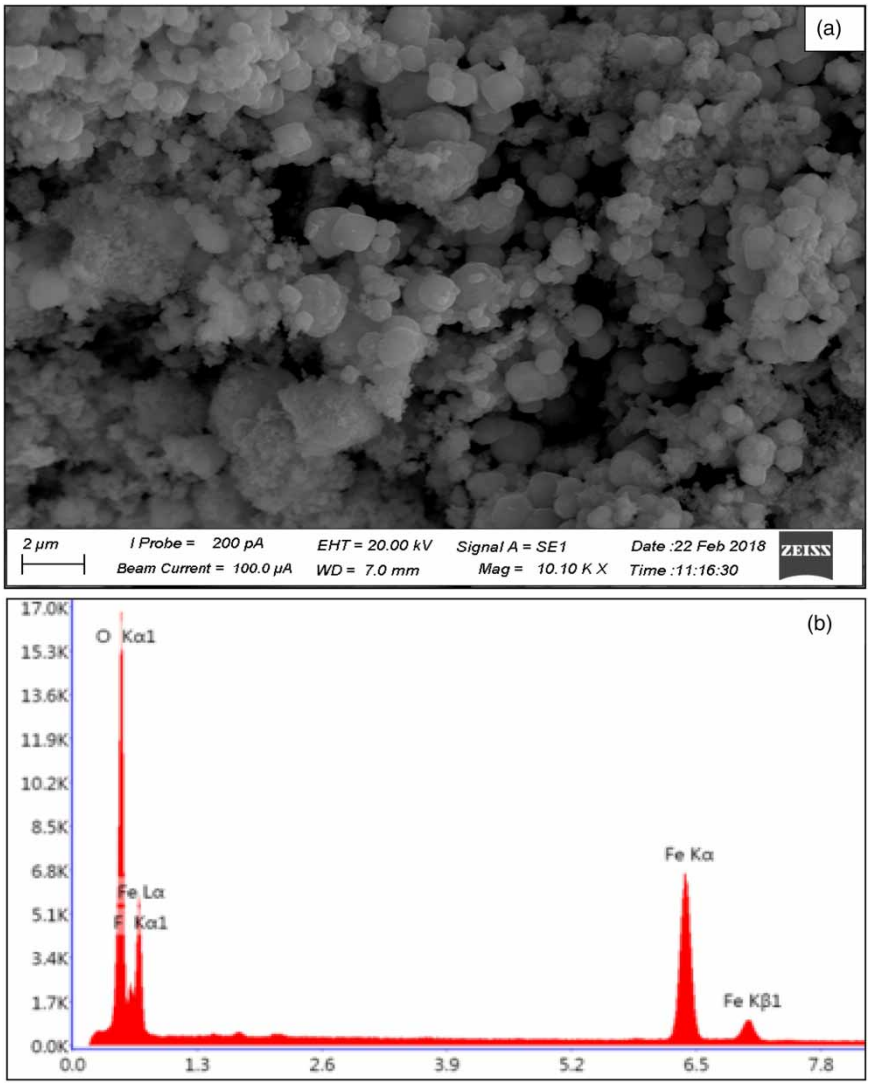

Figure 3 | Single-solute studies with fluoride (a) ESEM image of FeONs, and (b) EDX spectrum of FeONs (*Note*: EDX was performed on the whole surface area in Figure 3(a)).

ESEM-EDX analysis of CaF_2 (Figure 5(a) and 5(b)) shows that the CaF_2 formed was agglomerated and porous, with polycrystalline nanoparticles. The larger particles exhibited different, spherical, surface perturbations (Pandurangappa *et al.* 2010).

Water Practice & Technology Vol 14 No 3
doi: 10.2166/wpt.2019.052

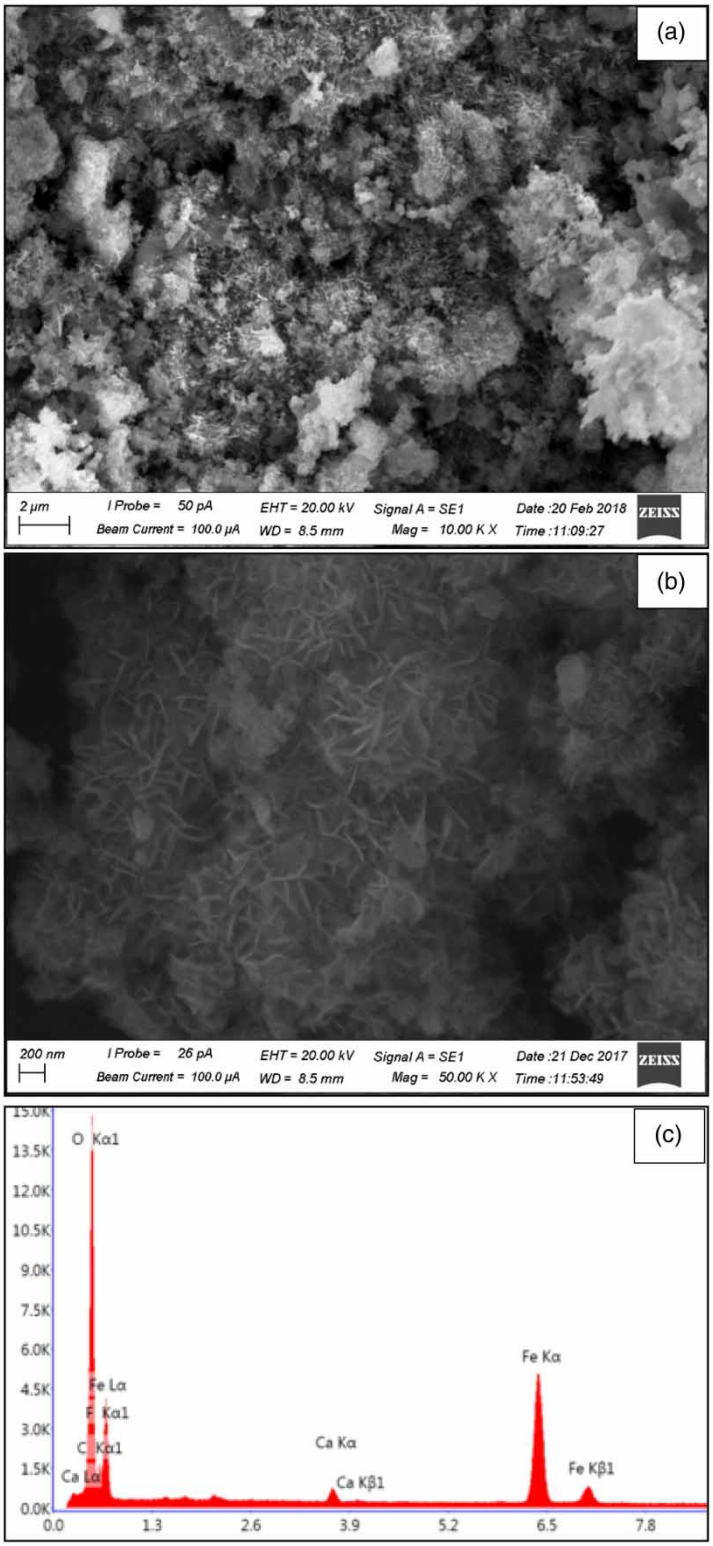

Figure 4 | Multi-solute studies with fluoride and calcium (a) ESEM image of FeONs, (b) ESEM image of FeON showing nodular-like patterns on the surface with Ca co-precipitation with FeONs (c) EDX spectrum of FeONs performed on the whole surface area in Figure 4(a).

FT-IR analysis

The FT-IR spectrum of FeONs shows both the specific peaks reflecting the surface functional groups and the surface's complex nature. Figure 6 shows the FT-IR spectrum of FeONs (a) before adsorption,

Water Practice & Technology Vol 14 No 3
doi: 10.2166/wpt.2019.052

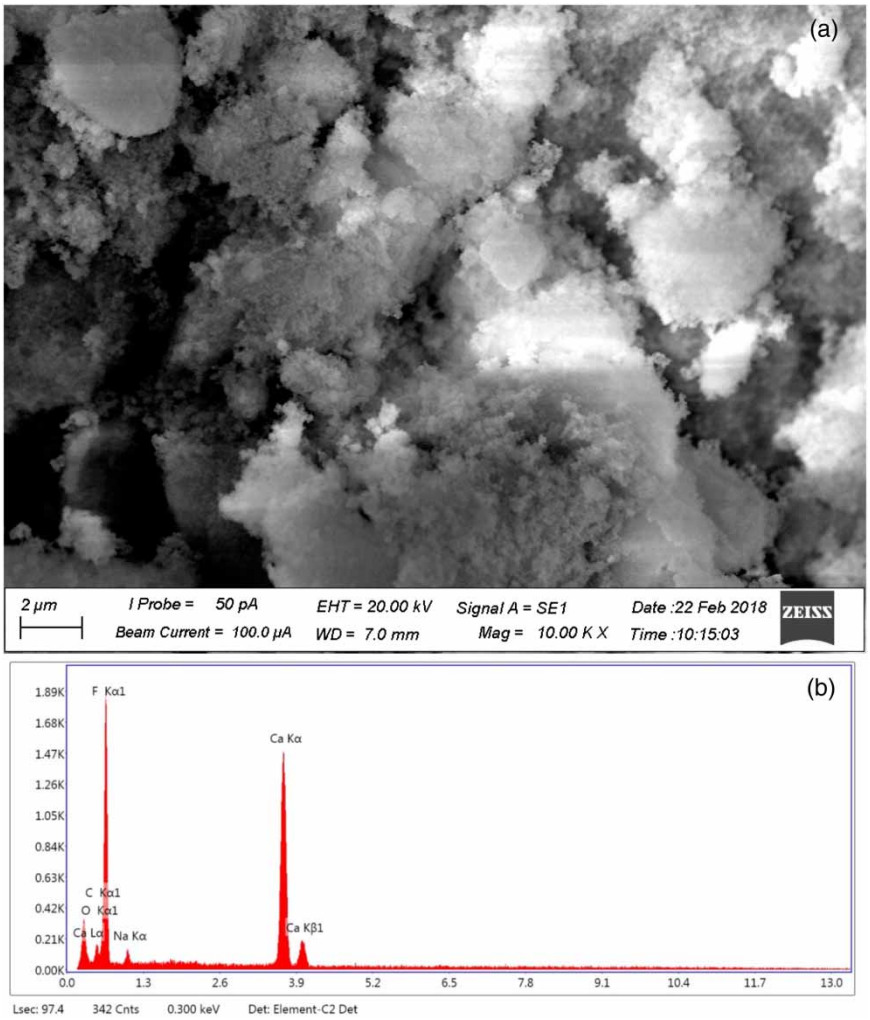

Figure 5 | Characterisation of CaF_2 formed in the binary mixture (a) ESEM image (b) EDX spectrum of CaF_2.

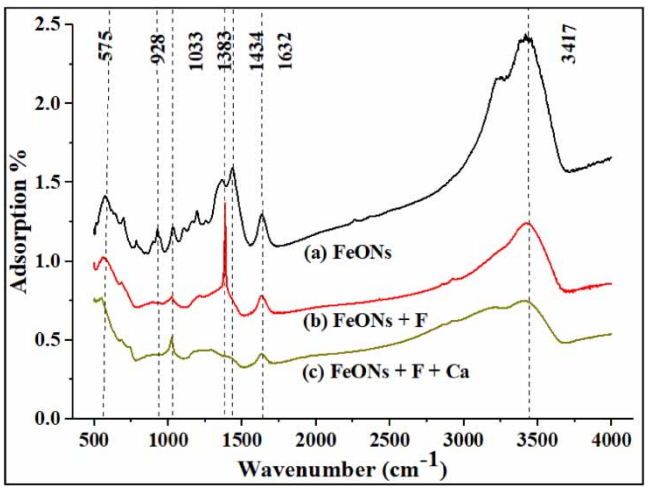

Figure 6 | FT-IR spectra of FeONs (a) before adsorption, (b) after fluoride adsorption (single-solute studies), and (c) after fluoride and calcium adsorption (multi-solute studies).

(b) after fluoride adsorption (single-solute studies), and (c) after fluoride and calcium adsorption (multi-solute studies). Before adsorption, there were broad bands around 1,033, 1,632, and 3,417 cm^{-1}, attributed to N–H and O–H bending, and O–H stretching vibrations, respectively (Sharma & Jeevanandam

Water Practice & Technology Vol 14 No 3
doi: 10.2166/wpt.2019.052

2013). N–H functional groups are indicated because of the use of NH_4OH solution to keep the pH between 10 and 11 during FeON synthesis. The band at 1,434 cm^{-1}, assigned to the symmetric and asymmetric bending of the C–H bond, may be ascribed to the ethanol added for FeON synthesis and storage (Qiu *et al.* 2011; Ayob & Abdullah 2012). The broad peak at 928 cm^{-1} arises from the bending vibrations of O–Fe–O groups (Jayarathna *et al.* 2015), and the narrow band around 575 cm^{-1} represents the Fe–O vibrations of magnetite nanoparticles (Xu *et al.* 2018).

After fluoride adsorption, the functional groups on the FeONs' surface had changed, and the broad peak around 3,000 to 4,000 cm^{-1} had weakened and shifted. The hydrogen-bonding strength was also diminished, and hydroxyl groups became much freer from their initial hydrogen-bonding character (Jayarathna *et al.* 2015), so that the new, isolated, surface –OH peak appeared around 3,824 cm^{-1}. The band at 1,632 cm^{-1} was shifted to 1,631 cm^{-1}, which was attributed to the presence of –OH groups even after fluoride adsorption onto FeONs (Jayarathna *et al.* 2015; Mohseni–Bandpi *et al.* 2015). The intensity of the band at 1,383 cm^{-1} was increased sharply, perhaps representing the characteristic peak of fluoride adsorption (Patnaik *et al.* 2016; Liu *et al.* 2018). The results generally indicate that the surface hydroxyl groups play a significant role in fluoride adsorption.

After fluoride and calcium adsorption, the broad peak at 3,417 cm^{-1} was decreased and shifted, with new peaks appearing at 3,406 and 3,205 cm^{-1}, attributed to the symmetric and asymmetric vibration of Fe–F and Fe–O–Ca–F bonds, respectively. A new peak appeared at 3,804 cm^{-1}, and the peak at 1,632 cm^{-1} was shifted to 1,630 cm^{-1}, indicating the presence of –OH groups after fluoride and calcium adsorption. In multi-solute adsorption, the sharp peak at 1,383 cm^{-1}, attributed to Fe–F bonding, was decreased and shifted, and a broad peak appeared assigned to the asymmetric F–Ca–O–Fe bridge. This might arise because calcium occupies the active sites available for fluoride, showing a new peak around 500 cm^{-1}, ascribed to Ca–O and Ca = O bonds (Galván-Ruiz *et al.* 2009) formed due to calcium adsorption and co-precipitation. The precipitation of CaF_2 in the multi-solute batch experiments could not be verified with FT-IR, as CaF_2's Ca–F stretching vibration occurs at 443 cm^{-1} (Tahvildari *et al.* 2012) – i.e., beyond the analytical range in this study.

Single-solute batch-studies

The possible mechanism of fluoride and calcium removal in single-solute batch-studies was identified as adsorption by FeONs. Therefore, attributes affecting fluoride and calcium adsorption by FeONs were studied.

Effect of FeON dosage, and initial fluoride and calcium concentrations on adsorption by FeONs

FeON dosage was varied from 0.04 to 7.20 g/L (Figure 7) to study its effect on fluoride and calcium adsorption. Fluoride adsorption showed little variation at FeON dosages exceeding 1.25 g/L, when it was 74%. Maximum calcium removal (39%) was observed at 1.25 g-FeONs/L with minor variation beyond that. For every FeON dosage, the total dissolved iron (Fe) concentration remaining after one-hour contact time with fluoride or calcium was measured by ion chromatography-mass spectrometry (ICP-MS) (Model: Agilent 7900 ICP-MS system, Japan, USA). The data showed that dissolution of Fe from the FeONs was less than 0.001 mg/L when dosage was increased, and that minute amounts of Fe dissolution did not affect FeON adsorption capacity. Increasing FeON dosage did, however, increase particle density per unit volume, increasing interaction between FeON particles and leading to agglomeration. This decreased the FeONs' adsorption capacity by decreasing the number of active sorption sites. Similar results have been reported for defluoridation with different adsorbent dosages of magnetite-chitosan composite (Mohseni-Bandpi *et al.* 2015).

The effect of initial concentration on fluoride adsorption was studied for the range 1 to 20 mg-F/L, over which fluoride adsorption increased from 0.04 to 5.3 mg/g. Calcium adsorption increased from

Water Practice & Technology Vol 14 No 3
doi: 10.2166/wpt.2019.052

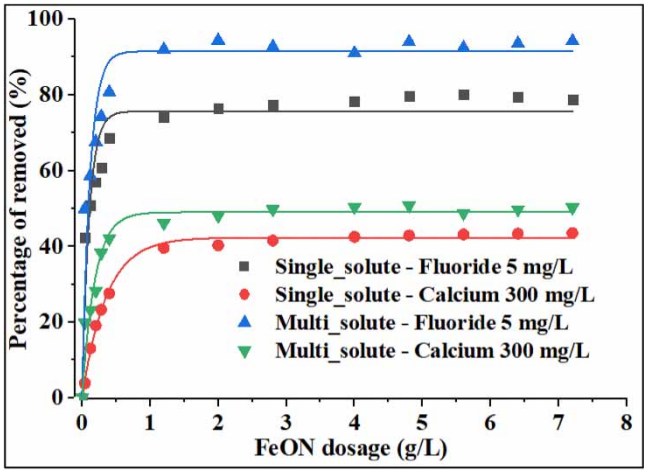

Figure 7 | Fluoride and calcium removal (%) vs FeON dosage in single-and multi- solute studies. The dosage was 1.25 g-FeON/L in all studies.

0.04 to 3.34 mg/g, at constant FeON dosage, for the initial calcium concentration range 100 to 500 mg-Ca/L.

Adsorption isotherms and kinetic models for fluoride and calcium

The equilibrium isotherm and kinetic model parameters for fluoride and calcium adsorption by FeONs are presented in Table 1. The R^2 values for the Langmuir isotherm adsorption model for both fluoride and calcium are 0.99, the high values indicating monolayer adsorption onto a surface with a finite number of active adsorption sites. The maximum monolayer adsorption capacities (Q_m) of FeONs based on the Langmuir model were 28.98 mg-F/g and 1.13 mg-Ca/g. The equilibrium parameter (R_L) was between 0.37 and 0.48 for fluoride, and 0.52 and 0.75 for calcium, indicating that the monolayer adsorption mechanism was favoured. The Freundlich constants (n) for fluoride and calcium were 1.35 and 1.79, respectively, indicating that F and Ca monolayer adsorption were moderately uncertain and weak, respectively. In single-solute batch experiments, monolayer adsorption

Table 1 | Adsorption isotherm parameters for fluoride and calcium adsorption on FeONs

		Adsorbed ions	
Isotherm model	**Parameter (units)**	**Fluoride**	**Calcium**
Langmuir	Q_m *(mg/g)*	28.98	1.13
	K_L *(L/mg)*	0.44	0.002
	R^2	0.99	0.99
Freundlich	K_f *(L/m)*	0.78	0.63
	1/n	0.74	0.56
	R^2	0.90	0.91
BET	Q_o *(mg/g)*	0.05	0.001
	K_b *(L/mg)*	46.95	0.39
	R^2	0.85	0.91
Temkin	A_T *(L/mg)*	0.40	7.58E-06
	B (J/mol)	0.10	3.41
	R^2	0.87	0.91
Dubinin-Radushkevich	Q_e *(mg/g)*	0.33	0.26
	E (KJ/mol)	1.80	0.01
	B_D *(mol^2/KJ)*	0.15	3,682.30
	R^2	0.93	0.75

Water Practice & Technology Vol 14 No 3
doi: 10.2166/wpt.2019.052

was, therefore, preferred for both species. The R^2 values for the BET adsorption isotherm for fluoride and calcium were 0.85 and 0.91, respectively, implying that the experimental data do not follow the BET isotherm assumption of multilayer formation during adsorption by FeONs. The equilibrium binding constant and adsorption energy variation for the Temkin model are given in Table 1. The Temkin model's R^2 values for F and Ca – 0.87 and 0.91, respectively – show that the model does not fit the experimental data well. The Dubinin-Radushkevich model's R^2 values for F and Ca were 0.93 and 0.75, respectively, showing that this model also failed to fit the experimental data well.

The adsorption kinetics of fluoride onto FeONs are described well by a pseudo-second-order model ($R^2 = 0.99$ to 1; Table 2). Hence, the rate-limiting factor of fluoride and calcium adsorption by FeONs is chemisorption, confirming covalent bonding by sharing or exchange of electrons between adsorbate and adsorbent (Arshadi *et al.* 2014). The results show that the experimental Q_e values ($Q_{e(Exp)}$) derived from the mass balance equation (Equation (1)) are approximately equal to the Q_e values calculated ($Q_{e(Cal)}$) with the pseudo-second-order equation (Equation (12)). As the experimental and calculated Q_e values are approximately equal, in single-solute batch-studies for both fluoride and calcium, adsorption was pronounced and removal due to co-precipitation could not be observed.

Table 2 | Equilibrium constants and thermodynamic parameters for kinetic models in single-solute studies

Pseudo-first-order					Pseudo-second-order			
Fluoride mg/L	**$Q_{e(exp)}$ mg/g**	**$Q_{e(Cal)}$ mg/g**	**K_1 min^{-1}**	**R^2**	**$Q_{e(Exp)}$ mg/g**	**$Q_{e(Cal)}$ mg/g**	**K_2 g/min/mg**	**R^2**
1	0.04	0.23	0.220	0.08	0.05	0.05	0.29	0.99
3	0.19	0.47	0.030	0.20	0.20	0.21	0.64	0.99
5	0.36	0.69	0.030	0.01	0.37	0.37	0.54	1.00
10	1.32	0.24	0.001	0.01	1.41	1.44	0.69	1.00
15	2.24	0.35	0.001	0.13	2.45	2.45	0.41	1.00
20	3.24	0.98	0.010	0.04	3.29	3.32	0.88	1.00
Calcium mg/L	**$Q_{e(Exp)}$ mg/g**	**$Q_{e(Cal)}$ mg/g**	**K_1 min^{-1}**	**R^2**	**$Q_{e(Exp)}$ mg/g**	**$Q_{e(Cal)}$ mg/g**	**K_2 g/min/mg**	**R^2**
200	0.48	0.25	−0.001	0.12	0.45	0.37	0.03	0.92
300	1.14	0.33	−0.006	0.33	1.78	1.80	0.17	0.99
400	2.38	0.05	−0.004	0.13	3.63	3.77	0.23	0.99
500	4.02	0.06	−0.002	0.25	5.98	6.01	0.25	0.99

Note: $Q_{e(Exp)}$ = experimental Q_e derived using the mass balance equation (*Equation (1)*); $Q_{e(Cal)}$ = calculated Q_e derived using the pseudo-second-order model.

Multi-solute batch-studies

The possible fluoride removal mechanisms in multi-solute batch-studies were identified as chemical precipitation as CaF_2 and adsorption by FeONs. For calcium removal they were identified as co-precipitation with oxide and hydroxide functional groups of FeONs, chemical precipitation as CaF_2 and adsorption by FeONs. Different physicochemical conditions in the mixture governed these mechanisms, so the potential for adsorption, co-precipitation and chemical precipitation was determined separately for different fluoride and calcium combinations.

Adsorption of fluoride and calcium by FeONs

The monolayer adsorption capacity of FeONs for fluoride and calcium removal was determined using constant 1.25 g-FeON/L dosage with different concentration combinations of fluoride and calcium (Figure 8). The fluoride and calcium concentrations were varied between 1.12 and 19.3 mg-F/L, and 136 and 980 mg-Ca/L, respectively. The monolayer adsorption capacity of fluoride for the

Water Practice & Technology Vol 14 No 3
doi: 10.2166/wpt.2019.052

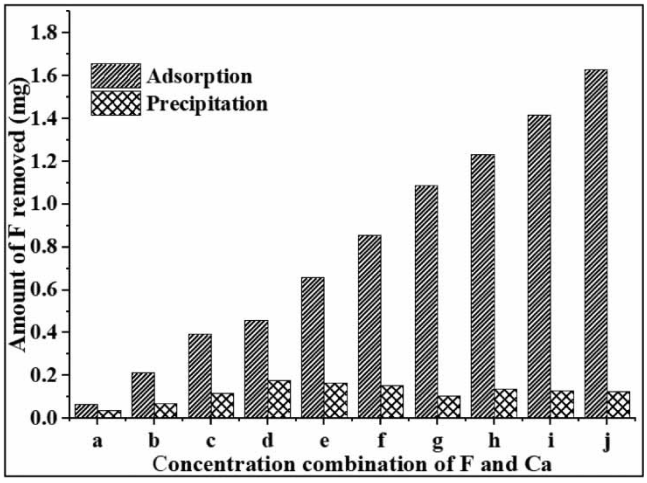

Figure 8 | Total fluoride removed by chemical precipitation and adsorption for different combinations of F and Ca. *Note:* For each combination in multi-solute batch-studies, the amounts of F and Ca (both as mg) used with solution volume 100 mL were (a) 0.11, 13.60 (b) 0.31, 22.00 (c) 0.56, 33.60 (d) 0.71, 40.40 (e) 0.91, 57.60 (f) 1.13, 66.00 (g) 1.32, 74.80 (h) 1.52, 83.20 (i) 1.71, 92.80, and (j) 1.93, 98.00.

corresponding combinations of fluoride and calcium, was between 0.07 and 1.63 mg for a 100 mL solution. For calcium it was between 0.29 and 0.49 mg (Figure 9). The results showed that for the combination containing 1.12 mg-F/L and 136 mg-Ca/L, total fluoride removal by FeONs occurred only through monolayer adsorption, with limited CaF_2 precipitation due to the low fluoride concentration. For other fluoride and calcium combinations, total fluoride removal was attributed to the formation of CaF_2 through chemical precipitation apart from some monolayer adsorption through chemisorption.

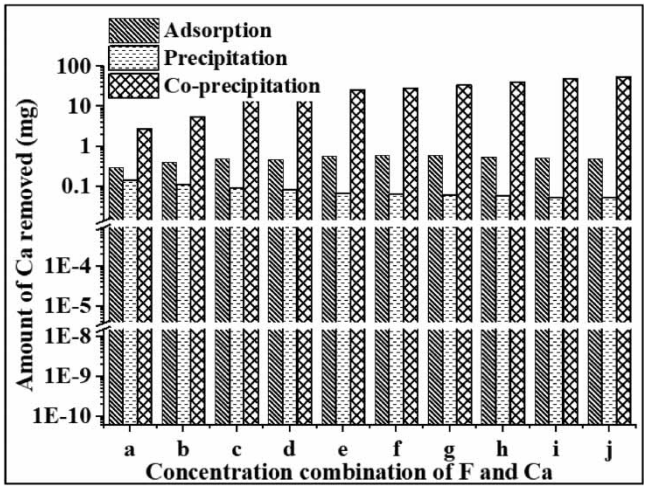

Figure 9 | Total calcium removed by co-precipitation, chemical precipitation and adsorption for different F and Ca combinations. *Note:* For each combination in multi-solute batch-studies, the amounts of F and Ca (both as mg) used with solution volume 100 mL were (a) 0.11, 13.60 (b) 0.31, 22.00 (c) 0.56, 33.60 (d) 0.71, 40.40 (e) 0.91, 57.60 (f) 1.13, 66.00 (g) 1.32, 74.80 (h) 1.52, 83.20 (i) 1.71, 92.80, and (j) 1.93, 98.00.

Chemical precipitation of CaF_2

Calcium and fluoride tend to form insoluble CaF_2 ($K_{sp} = 3.45 \times 10^{-11}$) via a stoichiometric reaction in the pH range 4.17 to 10 (Nasr *et al.* 2014). The solubility of CaF_2 is independent of pH above 4.17 but increases significantly at lower pH levels.

Water Practice & Technology Vol 14 No 3
doi: 10.2166/wpt.2019.052

Measurement of residual fluoride concentration temporal variations showed that much of the CaF_2 formed within an hour of mixing provided that the residual fluoride and calcium concentrations exceeded supersaturation levels. Similar observations were made by Nasr *et al.* (2014). Fluoride removal by chemical precipitation was in the range 0.04 to 0.13 mg for 100 mL of solution with increasing F and Ca levels (Figure 8). Therefore, total fluoride removal due to adsorption and chemical precipitation was determined as between 0.11 and 1.76 mg from corresponding initial fluoride concentrations of between 0.11 and 1.93 mg. The calcium content removed by chemical precipitation and co-precipitation was between 0.14 and 0.05 mg, and 2.76 and 55.46 mg, respectively, when F and Ca concentrations increased (Figure 9). Total calcium removal due to adsorption, chemical precipitation and co-precipitation was, therefore, in the range 3.20 to 56.00 mg, with initial calcium amounts between 13.60 and 98.00 mg. The difference between adsorption and co-precipitation depends mainly on the geometry of the adsorbate surface (Corey 1981), where co-precipitation is considered a 3-dimensional process leading to higher removal capacity than adsorption alone. The formation of mixed metal hydroxides, which is leading to enhanced metal ion removal at high orders of magnitude has been attributed to co-precipitation over adsorption (Crawford *et al.* 1993).

CONCLUSIONS AND RECOMMENDATIONS

Fluoride and calcium removal by FeONs in single-solute batch-studies was ascribed only to adsorption, and calcium co-precipitation was not observed. Adsorption studies suggested that both fluoride and calcium follow the Langmuir isotherm model and pseudo-second-order kinetics, indicating monolayer adsorption and chemisorption, respectively. The maximum monolayer adsorption capacities of FeONs were 28.98 and 1.13 mg/g for fluoride and calcium, respectively. In multi-solute batch-studies, fluoride removal was attributed to both adsorption and chemical precipitation as CaF_2 in almost similar magnitudes. For calcium removal in multi-solute batch-studies, co-precipitation, precipitation, and adsorption were the removal mechanisms, with co-precipitation the predominant contributor.

The study confirmed that FeONs are effective in removing fluoride by adsorption, in the absence or presence of calcium. Irrespective of the calcium concentration in raw water, the use of FeONs is worthwhile to lessen the combined effect of fluoride and calcium on CKDu.

CONFLICT OF INTEREST

No potential conflicts of interest were reported by the authors.

ACKNOWLEDGEMENTS

The Senate Research Committee (SRC) Grant of the University of Moratuwa (Grant No. SRC/ND/15/01) and the National Research Council (NRC), Sri Lanka (Grant No. 15-056) supported this research study.

REFERENCES

Arshadi, M., Amiri, M. J. & Mousavi, S. 2014 Kinetic, equilibrium and thermodynamic investigations of Ni(II), Cd(II), Cu(II) and Co(II) adsorption on barley straw ash. *Water Resources Industry* **6**, 1–17. doi.org/10.1016/j.wri.2014.06.001.

Ayob, A. & Abdullah, A. Z. 2012 Characterisation of polymer-stabilized nano zero-valent iron particle by ultrasonic irradiation-assisted method. *Journal of Polymer Materials* **29**, 167–179.

Water Practice & Technology Vol 14 No 3
doi: 10.2166/wpt.2019.052

Azzam, A. M., El-Wakeel, S. T., Mostafa, B. B. & El–Shahat, M. F. 2016 Removal of Pb, Cd, Cu and Ni from aqueous solution using nanoscale zero-valent iron particles. *Journal of Environmental Chemical Engineering* **4**(2), 2196–2206. doi.org/10.1016/j.jece.2016.03.048.

Barbier, O., Arreola-Mendoza, L. & Razo, D. L. M. 2010 Molecular mechanisms of fluoride toxicity. *Chemico-Biological Interaction* **188**(2), 319–333. doi:10.1016/j.cbi.2010.07.011.

Belkada, F. D., Kitous, O., Drouiche, N., Aoudj, S., Bouchelaghem, O., Abdi, N. & Mameri, N. 2018 Electrodialysis for fluoride and nitrate removal from synthesised photovoltaic industry wastewater. *Separation and Purification Technology* **204**, 108–115. doi.org/10.1016/j.seppur.2018.04.068.

Bhatnagar, A., Kumar, E. & Sillanpaa, M. 2011 Fluoride removal from water by adsorption – a review. *Chemical Engineering Journal* **171**(3), 811–840. doi:10.1016/j.cej.2011.05.028.

Brunauer, S., Emmett, P. H. & Teller, E. 1938 Adsorption of gases in multimolecular layers. *Journal of the American Chemical Society* **60**(2), 309–319.

Camacho, L. M., Dumée, L., Zhang, J., Li, J., Duke, M., Gomez, J. & Gray, S. 2013 Advances in membrane distillation for water desalination and purification applications. *Water* **5**(1), 94–196. doi:10.3390/w5010094.

Chandrajith, R., Padmasiri, J. P., Dissanayake, C. B. & Prematilaka, K. M. 2012 Spatial distribution of fluoride in groundwater of Sri Lanka. *Journal of the Natural Science Foundation of Sri Lanka* **40**(4), 303–309.

Chekli, L., Bayatsarmadi, B., Sekine, B. R., Sarkar, B., Shen, A. M., Scheckel, K. G., Skinner, W., Naidu, R., Shon, H. K., Lombi, E. & Donner, E. 2016 Analytical characterisation of nanoscale zero-valent iron: a methodological review. *Analytica Chimica Acta* **903**, 13–35. doi.org/10.1016/j.aca.2015.10.040.

Corey, R. B. 1981 *Adsorption of Inorganics at Solid-Liquid Interfaces* (Anderson, M. A. & Rubin, A. J. eds). Ann Arbor Science Publishers, Michigan, MI.

Crawford, R. J., Harding, I. H. & Mainwaring, D. E. 1993 Adsorption and co-precipitation of single heavy metals ions onto the hydrated oxides of iron and chromium. *Langmuir* **9**(11), 3050–3056.

Da Conceição, V. M., Ugri, M. C. B. A., Silveira, C., Nishi, L., Vieira, M. F., Bassetti, F. J., Vieira, A. M. S. & Bergamasco, B. 2015 Removal of excess fluoride from groundwater using natural coagulant *Moringa oleifera* lam and microfiltration. *The Canadian Journal of Chemical Engineering* **93**(1), 37–45.

Dharma-wardana, M. W. C. 2018 Chronic kidney disease of unknown aetiology (CKDu) and multiple-ion interactions in drinking water. *Environmental Geochemistry and Health* **40**(2), 705–719.

Dissanayake, C. B. & Chandrajith, R. 2017 Groundwater fluoride as a geochemical marker in the etiology of chronic kidney disease of unknown origin in Sri Lanka. *Ceylon Journal of Science* **46**(2), 3–12. doi.org/10.4038/cjs.v46i2.7425.

Dubinin, M. M. 1960 The potential theory of adsorption of gases and vapours for adsorbents with energetically non-uniform surfaces. *Chemical Reviews* **60**(2), 235–241.

Freundlich, H. M. F. 1906 Over the adsorption in solution. *Journal of Physical Chemistry* **57**, 385–471.

Galván-Ruiz, M., Hernandez, J., Banos, L., Noriega-Montes, J. & Rodríguez-García, M. E. 2009 Characterisation of calcium carbonate, calcium oxide, calcium hydroxide as starting point to the improvement of lime for their use in construction. *Journal of Materials in Civil Engineering* DOI: 10.1061/(ASCE)0899-1561(2009)21:11(694).

Gui, M., Smuleac, V., Ormsbee, L. E., Sedlak, D. L. & Bhattacharyya, D. 2012 Iron oxide nanoparticle synthesis in aqueous and membrane systems for oxidative degradation of trichloroethylene from water. *Journal of Nanoparticle Research* **14**(5), 861. DOI: 10.1007/s11051-012-0861-1.

Ho, Y. S. & McKay, G. 1999 Pseudo-second order model for sorption processes. *Process Biochemistry* **34**(5), 451–465.

Jadhav, S. V., Bringas, E., Yadav, G. D., Rathod, V. K., Ortiz, I. & Marathe, K. V. 2015 Treatment of fluoride concentrates from membrane unit using salt solutions. *Journal of Environmental Management* **162**(1), 306–325.

Jain, S. J. & Snoeyink, V. L. 1973 Adsorption from bi-solute systems on active carbon. *Water Pollution Control Federation* **45**(12), 2463–2479.

Jayarathna, L., Bandara, A., Ng, W. J. & Weerasooriya, R. 2015 Fluoride adsorption on $\gamma - Fe_2O_3$ nanoparticles. *Journal of Environmental Health Science and Engineering.* **13**, 54. DOI: 10.1186/s40201-015-0210-2.

Kakavandi, B., Jafari, A. J., Kalantary, R. R., Nasseri, S., Ameri, A. & Esrafily, A. 2013 Synthesis and properties of Fe_3O_4-activated carbon magnetic nanoparticles for removal of aniline from aqueous solution: equilibrium, kinetic and thermodynamic studies. *Iranian Journal of Environmental Health Sciences & Engineering* **10**(1), 19.

Lagergren, S. 1898 About the theory of so-called adsorption of soluble substances. *Kungliga Svenska Vetenskapsakademiens Handlingar* **24**, 1–39.

Langmuir, I. 1918 The adsorption of gases on plane surfaces of glass, mica and platinum. *Journal of the American Chemical Society* **40**(9), 1361–1403.

Lin, C. L., Lee, C. F. & Chiu, W. Y. 2005 Preparation and properties of poly (acrylic acid) oligomer stabilised superparamagnetic ferrofluid. *Journal of Colloid and Interface Science* **291**(2), 411–420.

Liu, J., Zhu, R., Xu, T., Laipan, M., Zhu, Y., Zhou, Q., Zhu, J. & He, H. 2018 Interaction of polyhydroxy fullerenes with ferrihydrite: adsorption and aggregation. *Journal of Environmental Sciences* **64**, 1–9. DOI: 10.1016/j.jes.2017.06.016.

Mohseni-Bandpi, A., Kakavandi, B., Kalantary, R. R., Azari, A. & Keramati, A. 2015 Development of a novel magnetite-chitosan composite for the removal of fluoride from drinking water: adsorption modelling and optimisation. *RSC Advances* **5**(89), 73279–73289. DOI: 10.1039/C5RA11294 J.

Water Practice & Technology Vol 14 No 3
doi: 10.2166/wpt.2019.052

Nasr, A. B., Walha, K., Puel, F., Mangin, D., Amar, R. B. & Charcosset, C. 2014 Precipitation and adsorption during fluoride removal from water by calcite in the presence of acetic acid. *Desalination and Water Treatment* **52**(10–12), 2231–2240. DOI: 10.1080/19443994.2013.799441.

Nath, S. K. & Dutta, R. K. 2010 Fluoride removal from water using crushed limestone. *Indian Journal of Chemical Technology* **17**(2), 120–125.

Pandurangappa, C., Lakshminarasappa, B. N. & Nagabhushana, B. M. 2010 Synthesis and characterisation of CaF_2 nanocrystals. *Journal of Alloys and Compounds* **489**(2), 592–595.

Patnaik, S., Mishra, P. C., Nayak, R. N. & Giri, A. K. 2016 Removal of fluoride from aqueous solution using chitosan-iron complex. *Journal of Analytical Bioanalytical Techniques* **7**, 326. DOI: 10.4172/2155-9872.1000326.

Petala, E., Dimos, K., Douvalis, A., Bakas, T., Tucek, J., Zboril, R. & Karakassides, M. A. 2013 Nanoscale zero-valent iron supported on mesoporous silica: characterization and reactivity for Cr(VI) removal from aqueous solution. *Journal of Hazardous Materials* **261**, 295–306.

Qiu, X., Fang, Z., Liang, B., Gu, F. & Xu, Z. 2011 Degradation of decabromodiphenyl ether by nano zero-valent iron immobilised in mesoporous silica microspheres. *Journal of Hazardous Materials* **193**, 70–81.

Raul, P., Umlong, I. M. & Purkait, M. K. 2012 Removal of fluoride from water using iron oxide-hydroxide nanoparticles. *Journal of Nanoscience and Nanotechnology* **12**(5), 3922–3930. DOI: 10.1166/jnn.2012.5870.

Robshaw, T., Dawson, R., Bonser, K. & Ogden, M. D. 2019 Towards the implementation of an ion-exchange system for recovery of fluoride commodity chemicals. Kinetic and dynamic studies. *Chemical Engineering Journal* **367**, 149–159. doi.org/10.1016/j.cej.2019.02.135.

Sharma, G. & Jeevanandam, P. 2013 Synthesis of self-assembled prismatic iron oxide nanoparticles by a novel thermal decomposition route. *RSC Advances* **3**(1), 189–200. DOI: 10.1039/c2ra22004 k.

Shukla, S., Jadaun, A., Arora, V., Sinha, R. K., Biyani, N. & Jain, V. K. 2015 In vitro toxicity assessment of chitosan oligosaccharide coated iron oxide nanoparticles. *Toxicology Report* **2**, 27–39.

Tahvildari, K., Pour, M. E., Ghammamy, S. & Nabipour, H. 2012 CaF_2 nanoparticles: synthesis and characterisation. *International Journal of Nano Dimension* **2**(4), 269–273.

Tempkin, M. I. & Pyzhev, V. 1940 Kinetics of ammonia synthesis on promoted iron catalyst. *Acta Physico-Chimica Sinica* **12**, 327–356.

USEPA 1983 Methods for chemical analysis of water and waste, Report EPA/600/4-79/020, Environmental Monitoring and Support Laboratory, Office of Research and Development, United State Environmental Protection Agency, Cincinnati, Ohio, Washington.

Wasana, H. M. S., Aluthpatabendi, D., Kularatne, W. M. T. D., Wijekoon, P., Weerasooriya, R. & Bandara, J. 2016 Drinking water quality and chronic kidney disease of unknown etiology (CKDu): synergic effects of fluoride, cadmium and hardness of water. *Environmental Geochemistry and Health* **38**(1), 157–168. DOI 10.1007/s10653-015-9699-7.

Weber, T. W. & Chakravorti, R. K. 1974 Pore and solid diffusion models for fixed bed adsorbers. *AIChE J.* **20**(2), 228–238.

Weragoda, S. K. & Kawakami, T. 2017 Evaluation of groundwater quality in 14 districts in Sri Lanka: a collaboration research between Sri Lanka and Japan. In: *Trends in Asian Water Environmental Science and Technology* (Kurisu, F., Ramanathan, A. L., Kazmi, A. A. & Kumar, M. eds). Springer International Publishing, Cham, Switzerland and Capital Publishing Company, New Delhi, India, pp. 151–155.

WHO (World Health Organisation). 2017 *Guidelines for Drinking Water Quality: 4th Edition Incorporating the 1st Addendum*. Geneva, World Health Organization, CC BY-NC-SA 3.0 IGO.

Wu, S., Sun, A. & Zhai, F. 2011 Fe_3O_4 magnetic nanoparticles synthesis from tailings by ultrasonic chemical co-precipitation. *Materials Letters* **65**(12), 1882–1884.

Xu, J., Yang, H., Fu, W., Du, K., Sui, Y., Chen, J., Zeng, Y., Li, M. & Zou, G. 2007 Preparation and magnetic properties of magnetite nanoparticles by sol-gel method. *Journal of Magnetism and Magnetic Materials* **309**(2), 307–311. doi.org/10.1016/j.jmmm.2006.07.037.

Xu, C., Yang, W., Liu, W., Sun, H., Jiao, C. & Lin, A. 2018 Performance and mechanism of Cr (VI) removal by zero-valent iron loaded onto expanded graphite. *Journal of Environmental Sciences* **67**, 14–22. doi.org/10.1016/j.jes.2017.11.003.

Zager, R. A. & Iwata, M. 1997 Inorganic fluoride divergent effects on human proximal tubular cell viability. *American Journal of Pathology* **150**(2), 735–743. PMC1858266.